Int. J. Electrochem. Sci., 7 **(2012)** 9325 - 9344

International Journal of ELECTROCHEMICAL SCIENCE
www.electrochemsci.org

Sub-Microscopic Phenomena of Metallic Corrosion Studied by a Combined Photoelectron Spectroscopy in Air (PESA) and Scanning Kelvin Probe Force Microscopy (SKPFM) Approach

Tongyan Pan [1,*], *and Lu Sun* [1]

[1] Department of Civil Engineering, The Catholic University of America, 620 Michigan Avenue, N.E., Washington, DC, 20064.
* E-mail: pan@cua.edu.

Received: 10 July 2012 / *Accepted:* 31 August 2012 / *Published:* 1 October 2012

The management of metallic corrosion has relied on large-scale, ultra-conservative protection strategies such as the extensive use of anti-corrosion metals and alloys, all-inclusive coating and surface passivation, and substantial use cathodic protection. In the current state of knowledge, the corrosion durability of technically protected metallic materials is controlled by the chemical or structural heterogeneous inclusions in the metallic matrix, which play a key role in being potential initiation sites of pitting, crevice, or filiform corrosion. This status quo demands a well-developed capability to precisely track the sub-microscopic corrosion phenomena, which however is beyond the resolution and accuracy capacities of standard electrochemical techniques. Different from the conventional electrochemical approaches, an innovative approach is developed in this study by directly measuring the absolute electrode potential E_{abs} on a metallic surface that can be accomplished at the sub-microscopic resolution and accuracy. E_{abs} of a specific solid-state metallic material or phase, which is believed to be practically immeasurable in classical electrochemistry, includes two contributing components, i.e., the work function of the material and the Volta potential difference between the material and the aqueous electrolyte covering its surface. With the state-of-the-art surface analytical techniques, i.e., the Photoelectron Spectroscopy in Air (PESA) and Scanning Kelvin Probe Force Microscopy (SKPFM), the two components today can be readily measured at the atomic-level resolution and accuracy. The coupled PEESA and SKPFM approach also allows the measurement E_{abs} of metallic surfaces covered by oxides, water molecules and/or coating materials as well as determining the physical changes and integrity of the cover materials, therefore allows for in-situ studying of sub-microscopic corrosion phenomena under a wide variety of in-service conditions.

Keywords: Metallic Corrosion, Sub-Microscopic Phenomena, PESA, SKPFM

1. INTRODUCTION

General civil and military engineering practices demand high-performance metallic materials that offer superior strength and toughness, extraordinary corrosion resistance, light weight, and the ability to maintain these properties at extreme temperatures. Although some precious metallic materials like titanium alloys possess inclusively these desired properties, they are not commonly used in practice due to the high cost of raw materials and/or processing. In reality, relatively low-cost materials, particularly the steels and aluminum alloys, have been used as the major structural materials.

Meeting the general mechanical, temperature and/or light-weight needs, steels and aluminum alloys however are not immune to corrosion, a thermodynamically spontaneous phenomenon occurring to most metallic materials under general service conditions. Metallic corrosion, referred to as the deterioration of metals and alloys or their useful properties by reaction with the working environment, takes two general modes according to the contributing factors, i.e., the general corrosion (non-stress related) and stress-related corrosion, both being able to occur in atmospheric, immersion, and alternate immersion conditions. General carbon steels, mainly used as structural steels, suffer mainly from the general corrosion, while most stainless steels are prone to stress-related corrosion [1, 2]. High-strength aluminum alloys such as AA2024-T3 are commonly used in aircrafts owing to their light weights. Aluminum alloys however in general are susceptible to localized corrosion in chloride-containing or marine environments, as a result of the intermetallic particles introduced during cooling solidification or intentionally developed for optimized mechanical properties, such as the copper-containing particles [3].

Once started, metallic corrosion and the incurred material and structural degradations are rather tough to remedy, and the incurred treatment cost can easily exceed the cost of replacement or re-building. According to some recent studies, corrosion costs the U.S. Department of the Navy an amount of $3.2 billion each year only on ships, which is about 26.3 percent of its annual maintenance cost [4-6]. More unaffordably, the repair and replacement activities frequently take critical systems out of service condition, leading to reduced mission readiness [7]. Also, corrosion can pose severe safety threats when a corroded component(s) causes the failure of the entire system in operation, such as the corroded electrical contacts in a flying aircraft [5, 6].

Building on the classical thermodynamics-based electrochemistry that has been developed and therefore holds its validity for general macroscopic phenomena, the current practices of corrosion management depend on large-scale, ultra-conservative protection strategies such as extensive use of anti-corrosion metals and alloys, all-inclusive coating and surface passivation, and substantial use cathodic protection to ensure the high-standard service conditions of its military assets. These strategies however usually entail high initial investment (e.g., the use of corrosion-resistant alloys), significant maintenance cost (e.g., the use of coatings), or both (e.g., the use of cathodic protection). In the current state of knowledge, the corrosion durability of technically protected metallic materials, such as coated or passivated carbon steels, stainless steels or aluminum alloys, is controlled by the chemical or structural heterogeneous inclusions in the metallic matrix, which play a key role in being potential initiation sites of pitting, crevice or filiform corrosion [1-3, 8, 9-21].

Without proper considerations given to the sub-microscale phenomena, the existing corrosion management strategies have constantly been subject to unexpected problems. For example, the stainless steels originally used to resist general corrosion were later on found to be susceptible to stress-related corrosion due to the unique microstructures and intermetallic materials formed in metallic matrix. Coatings play a major role in combatting corrosion and have received particular attention. Today nearly all naval ships, submersible, amphibious and land-based vehicles, aircraft, and hypersonic vehicles are coated with organic, polymer or metallic materials. Coatings, although providing immediate protection, in general are subject to early deteriorations due to the vulnerability of coating materials and/or coating-substrate interface. Regarding the protection mechanisms of coatings however, it usually is not the direct barrier effect on the diffusion process that gives rise to the corrosion stability, but the specific electrochemical properties of the metal-coating interface, in particular, the formation of an extended nanoscale diffusion double layer [22]. Filiform corrosion, a common type of corrosion occurring to coated metallic materials such as steels and aluminum alloys, is an example in this regard.

Within this context, in today's practice of corrosion management, critical information is missing in the sub-microscale domain. Such information include but not limited to 1) surface corrosion potential and passivity of metallic grains, grain boundaries, and heterogeneous precipitations or inclusions, which essentially control the formation of microscopic corrosion cells in pitting, crevice and filiform corrosion, 2) behavior of electric double layer at the coating-solution and metal-solution interfaces, which is closely related to the corrosion rate and the effectiveness and longevity of coatings or inhibitors, and 3) stress and strain effects on distribution of surface corrosion potential among different phases, which determines the stress-related corrosion behavior of metallic materials. Such sub-microscopic information is critical for early detection of corrosion, monitoring of corrosion rate and deterioration severity, evaluation of corrosion protection strategies such as coating, and development of new materials, novel corrosion protection techniques, and best management practices (BMP) for corrosion management.

2. METHODOLOGY DESCRIPTION

Conventional electrochemical methods to study localized corrosion are based on large-scale experiments with exposed surface areas in the square-millimeter (size of a reference electrode tip) to square-centimeter range (typical size of a sample in full-scale tests). Electrochemical corrosion tests on samples of a few square centimeters or millimeters provide information only on the behavior of a large material surface, i.e., the macroscopic corrosion behavior, as such area sizes are large enough to cover multiple grains, grain boundaries, precipitations and other inclusions. Therefore the conventional electrochemical methods are not suitable for studying localized corrosion processes, whether free (unprotected) or protected by coating or passivation techniques, such as the pitting corrosion and filiform corrosion, respectively [23].

Therefore, alternative electrochemical techniques are needed for corrosion studies in the micron and sun-microscopic (≤ 1 □m) range that permit reducing the diameter of the exposed surface

to ≤ 1 square □m to isolate the phases of metallic grains, grain boundaries, precipitations and other inclusions, and make it possible to detect the different corrosion behavior of the single heterogeneities in metallic matrix. Such investigations can lead to an insight into the initiation mechanism of localized corrosion, if they can be performed under the in-situ corrosion condition.

Electrochemical techniques that have been used for localized corrosion tests in the sub-microscopic dimensions can be divided into two major groups: 1) Scanning techniques—by scanning an immersed samples using microelectrodes or nanoelectrodes to obtain information in the local distribution of one or several parameters during corrosion experiments; 2) Small-area techniques—by decreasing the size of the exposed corrosion surface to localize the electrochemical process, which can be achieved by thin embedded wires, photoresist techniques, a droplet cell, or small glass capillaries touching only small areas of the specimen surface. Scanning-mode experiments can be performed under open-circuit conditions or under potential or current control, and depending on the particular technique a lateral resolution down to a few nanometers can be reached. The small-area techniques on the other hand allow polarization of microscopic surface areas, and with a high-resolution potentiostat to record the corrosion processes at a molecular level.

Recent advances in surface physicochemical analyses enable high-resolution determination of surface electrode or corrosion potential and topography of generic metallic materials, which opens a new avenue for accurately studying the sub-microscale phenomena involved in metallic corrosion. Of the various modern techniques, two are especially suitable for the purpose of studying sub-microscopic corrosion phenomena under the in-situ conditions, i.e., the Photoelectron Spectroscopy in Air (PESA) that is capable of measuring the work function of a bare, passivated, or coated metallic surface, and the Scanning Kelvin Probe Force Microscopy (SKPFM) that is capable of mapping the Volta potential of a bare, passivated, or coated metallic surface, both at the atomic-level accuracy. Hence through the combined use of PESA and SKPFM, the absolute electrode potential as the sum of work function and Volta potential can be readily determined at specific locations in the different metallic grains, grain boundaries, and heterogeneous inclusions of a metallic surface. The absolute electrode potential at different locations on a metallic surface collectively will present a sub-microscopic map of corrosion potential of the surface.

Furthermore, based on the measured signal in the work function of substrate metal or alloy, PESA can determine the thickness of passive oxide film covering the substrate by measuring the number of atomic layers in the film up to a few tens of nanometers in thickness; therefore it can be used to monitor the growth rate of corrosion products, i.e., the corrosion rate on the metallic surface that can be ensured at the atomic-level accuracy. SKPFM, when using its atomic force microscopy mode, also can determine the topology of a metallic surface and be used to accurately study the rate of corrosion. Equally importantly, SKPFM can detect potential under an organic or polymer layer up to hundreds of microns in thickness, and can be used to study coated or inhibited corrosion phenomena such as filiform corrosion.

Therefore in combination the PESA and SKPFM techniques allow for in-situ studying of a wide spectrum of sub-microscopic corrosion phenomena, whether in unprotected, protected, atmospheric, or immersion types of corrosion. Such unique capacities enable, for the first time, a fundamental understanding of the sub-microscopic mechanisms of corrosion phenomena, a

comparative study of the stress and strain effects, and a high-accuracy evaluation of the effectiveness and longevity of existing and new coating materials and techniques under the in-service conditions. These advantages of the developed sub-microscopic study can significantly enhance the capabilities in analyzing and controlling corrosion related problems at reduced cost.

2.1. Theoretical Background of the Innovative Methodology

Critical to the sub-microscopic study of metallic corrosion is the accurate measurement of in-situ absolute electrode potential E_{abs} at a high lateral resolution (sub-microscopic), which when available can be used to determine the corrosion potential that actually drives the electrode reactions on a metallic surface. The absolute electrode potential E_{abs} of a metallic sample covered by a liquid electrolyte layer, according to the significant work by Trasatti [15, 24, 25], can be defined as the minimum potential needed to transfer an electron from the Fermi level of the sample, through the solid/liquid interface (with a potential drop of $\Delta\varphi_M^{El}$), the liquid, and the liquid surface to a position just outside the liquid (Path A→C in Figure 1-a).

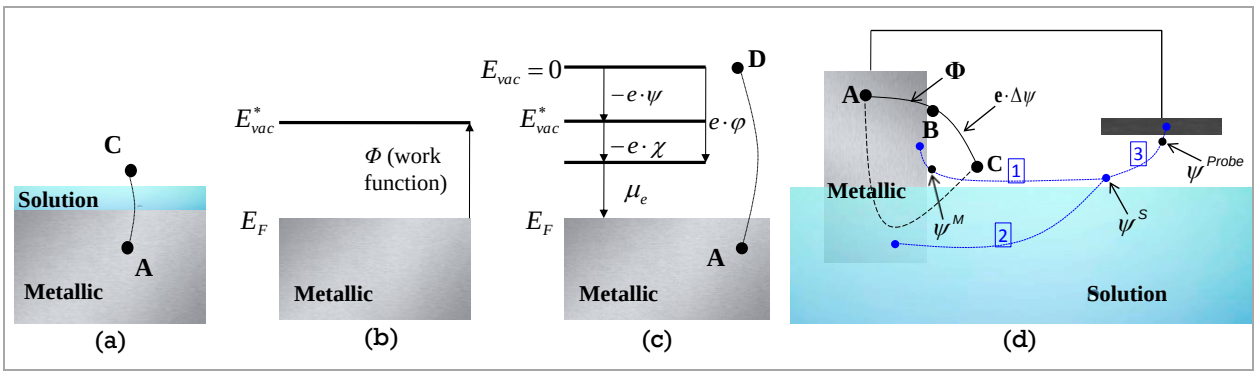

Figure 1. Schematic Illustration of the Absolution Electrode Potential E_{abs} on a Metallic Surface

According to the definition, the absolute electrode potential can be formulated based on the concept of *work function* Φ of a metallic sample, which is the minimum work required for extracting an electron from inside the sample to a position just outside the sample that is far enough to eliminate contributions from image forces (see Figure 1-b) [15, 24, 25]. Work function is equivalent to the difference in energy between the vacuum level and Fermi level indicated in Figure 1-b as E_{vac}^* and E_F, respectively. Work function Φ therefore consists of two parts per Eq. (1) for a sample that carries no net electrical charges, i.e., the chemical work μ_e — the chemical energy needed to transfer the electron from the infinity into the sample, and the dipole or surface potential related work $e\chi$ that takes into account the electrostatic work to transport the electron through the dipole layer of sample surface, where χ is the potential drop between just inside the bulk material and just outside of it [24].

$$\Phi = -\mu_e + e\chi = -(\mu_e - e\chi) \qquad (1)$$

For general objects that carry a net electrical charge such as a metallic phase of a sample in corrosion studies, an additional work term is needed to transfer the electron from just outside the sample surface to a position in absolute vacuum or infinitely far away (see Figure 1-c). The additional component can be calculated as $e\psi$, with which a *generalized work function* Φ^* can be defined per Eq. (2) as the work required for extracting an electron from within the sample (Point A in Figure 1-c) to infinitely far away, for example the Point B in Figure 1-c in the absolute vacuum. The symbol ψ is the Volta potential which is equivalent to the potential drop from infinitely far away to a location just outside the surface.

$$\Phi^* = -\mu_e + e\chi + e\psi = -(\mu_e - e\chi - e\psi) \quad (2)$$

The sum of the dipole/surface potential χ and Volta potential ψ gives the Galvani potential □, which is the potential drop between the bulk sample and the vacuum level infinitely far away from the surface.

$$\varphi = \chi + \psi \quad (3)$$

The absolute electrode potential E_{abs} of a sample covered by a liquid layer can be defined, based on the concept of the generalized work function, as the minimum potential needed to transfer an electron from the Fermi level, through the solid/liquid interface (with the potential drop of $\Delta\varphi_M^{El}$), the liquid and its surface layer to a position just outside the liquid, following the Path A→C (dashed curve) in Figures 1-a and 1-d. E_{abs} per Eq. (4) then can be formulated based on Eq. (1) by adding an additional term $\Delta\varphi_M^{El} = \varphi_M - \varphi_{El}$, the potential drop at the metal/liquid interface (with "*El*" means "electrolyte"), and replacing the χ with the dipole/surface potential of the liquid surface χ_S. Φ_{M-S}^* is the generalized work function of an electron that is transferred following the path A→C (dashed curve), i.e., from within the sample or an electrode to a position outside the liquid layer covering the sample [15, 24, 25].

$$E_{abs} = \frac{1}{e}\Phi_{M-S}^* = (-\frac{\mu_e}{e} + \Delta\varphi_M^{El} + \chi_S) \quad (4)$$

According to Figure 1-d, if an electron is transferred along the path A→B→C (solid curve) instead of A→C (dashed curve), Eq. (5) can be obtained, with Φ being the work function, and ψ^M - ψ^S = $\Delta\psi$ being the Volta potentials difference between one point outside the metallic sample and one point outside the solution.

$$E_{abs} = \frac{1}{e}\Phi + (\psi^M - \psi^S) \quad (5)$$

Based on the concept of absolute electrode potential, if a second metallic sample, such as an electrode or a scanning probe, is connected to the first metallic sample by a metallic wire and positioned near the surface of the electrolyte as shown in Figure 1-d, Eq. (6) can be obtained, with the

three terms after the three equal marks corresponding to the three paths 1, 2, and 3 shown in the figure, considering that the work function difference between any point inside the metallic system i.e., the two metallic samples connected by a metallic wire, and a point right outside of the electrolyte (liquid solution) is a fixed value no matter what path is taken. The symbols ψ^{Probe} and ψ^{S} are the Volta potentials at a point outside the metallic probe and a point outside the solution, respectively. Notably, the work required to transfer an electron between two metal samples via a metallic wire is negligible.

$$\begin{aligned} E_{abs} &= \frac{1}{e}\Phi^{*}_{M-S} \\ &= (-\frac{\mu_e}{e} + \Delta\varphi^{El}_{M} + \chi_S) \\ &= \frac{1}{e}\Phi^{M} + (\psi^{M} - \psi^{S}) \\ &= \frac{1}{e}\Phi^{Probe} + (\psi^{Probe} - \psi^{S}) \end{aligned} \tag{6}$$

Therefore, the absolute electrode potential of a specific solid-state metallic material or phase, in a corrosive condition, includes two contributing components, i.e., the work function of the materials and the Volta potential difference between the metallic material and the electrolyte covering its surface. In classical electrochemistry however, the absolute electrode potential that include the potential change cross a "single" electrode-solution interface cannot be measured by standard electrochemical techniques [24]. Therefore to date the electrode potential or corrosion has been measured with respect to a reference electrode such as the standard hydrogen electrode (SHE), saturated calomel electrode (SCE), or Ag/AgCl electrodes that in measurement operations have to bring in an additional electrode-solution interface.

Different from the classical electrochemical methods, an innovative approach is developed in this study by directly measuring the absolute electrode potential E_{abs} on a metallic surface that can be conducted at the atomic spatial resolution and accuracy, i.e., by measuring the E_{abs} of each different metallurgical or compositional phase of a multi-inclusion metallic surface at the sub-microscopic resolution and accuracy that cannot be reached by the classical electrochemical methods. To this end, the last two equations in Eq. (6) i.e., $\frac{1}{e}\Phi^{M} + (\psi^{M} - \psi^{S}) = \frac{1}{e}\Phi^{Probe} + (\psi^{Probe} - \psi^{S})$ can be re-organized to be Eq. (7-a), with the term ψ^{S} cancelled from both sides. The work function of the metallic surface Φ^{M} in Eq. (7-a), or the Φ_i^{M} in Eq. (7-a-1) of the i^{th} phase of the metallic surface, can be directly measured by the PESA technique. The Volta potential difference of the metallic surface $(\psi^{M} - \psi^{Probe})$, or the $(\psi_i^{M} - \psi_i^{Probe})$ in Eq. (7-a-1) of the i^{th} phase of the metallic surface, can be directly measured by the SKPFM technique. Based on these direct measurements, the work function of the metallic probe Φ^{Probe} or Φ_i^{Probe} in Eq. (7-a) or (7-a-1) can be determined.

$$\frac{1}{e}\Phi^{Probe} = \frac{1}{e}\Phi^{M} + (\psi^{M} - \psi^{Probe}) \tag{7-a}$$

$$\frac{1}{e}\Phi_i^{Probe} = \frac{1}{e}\Phi_i^{M} + (\psi_i^{M} - \psi_i^{Probe}) \quad (7\text{-a-1})$$

$$E_{abs} = \frac{1}{e}\Phi^{Probe} + (\psi^{Probe} - \psi^{S}) = \frac{1}{e}\Phi^{M} + (\psi^{M} - \psi^{Probe}) + (\psi^{Probe} - \psi^{S}) \quad (7\text{-b})$$

$$E_{abs,i} = \frac{1}{e}\Phi_i^{Probe} + (\psi_i^{Probe} - \psi_i^{S}) = \frac{1}{e}\Phi_i^{M} + (\psi_i^{M} - \psi_i^{Probe}) + (\psi_i^{Probe} - \psi_i^{S}) \quad (7\text{-b-1})$$

Then, the absolute electrode potential of a metallic surface, E_{abs}, or the i^{th} phase of the metallic surface, $E_{abs,i}$, can be determined per Eq. (7-b) and Eq. (7-b-1) that are derived directly from the last equation in Eq. (6), with the Volta potential difference $(\psi^{Probe} - \psi^{S})$ and $(\psi_i^{Probe} - \psi_i^{S})$ in Eqs. (7-b) and (7-b-1) also directly measured by the SKPFM technique. It must be pointed out that the right-hand side of Eqs. (7-b) and (7-b-1) look the same as the term $\frac{1}{e}\Phi^{M} + (\psi^{M} - \psi^{S})$ in Eq. (6) if the term ψ^{Probe} is cancelled; however, such format as Eqs. (7-b) or (7-b-1) are necessary since experimentally only the terms $(\psi^{Probe} - \psi^{S})$ and $(\psi_i^{Probe} - \psi_i^{S})$ but not the term $(\psi^{M} - \psi^{S})$ can be measured (using SKPFM).

Notably, this new approach involves direct measurements of the work function of a metallic surface and the Volta potential difference between the metallic surface and the electrolyte covering the metallic surface, both at the atomic-level resolution and accuracy (using the state-of-the-art surface analysis techniques PESA and SKPFM). Hence this approach involves three steps, i.e., 1) measuring surface work function using PESA, 2) measuring Volta potential difference using SKPFM, and 3) coupling the PESA and SKPFM measurement to obtain the absolute electrode potential. For general metallic materials like steels and aluminum alloys, each as a multi-phase composite, a high-resolution and high-accuracy absolute $E_{abs,i}$ map determined in their pre- or early corrosion period provides an ideal platform to study the imitation mechanisms of corrosion. More importantly, the method can be used to study the stress/strain effects and the mechanisms of various corrosion protection strategies such as coatings, cathodic protection, and corrosion inhibitors.

2.2. High-Resolution Measurement of Work Function by PESA

The existing experimental methods developed to measure the work function of a metallic sample can be classified in two groups [23]: the absolute methods and the relative methods. Methods of the first group employ electron emission from the sample induced by photon absorption (photoemission), high temperature (thermionic emission), electric field (field electron emission), or using electron tunneling. The relative methods, on the other hand, make use of the contact potential difference between the sample and a probe or reference electrode. Experimentally, an anode current of a diode is used or the displacement current between the sample and reference (created by an artificial change in the capacitance between the two) is measured [23].

The photoelectron spectroscopy (PES) methods for determining work function are based on the outer photoelectric or photoemission effect. The sample surface is exposed to a beam of photons such as by ultraviolet (UV) light that can induce photoelectric ionization. The energies of the emitted

photoelectrons are characteristic of their original electronic states, and depend also on vibrational state and rotational level. In the case of Ultraviolet Photoelectron Spectroscopy (UPS), the surface of a solid sample is irradiated with UV light and the kinetic energy of the emitted electrons (called photoelectrons) is analyzed. As UV light is electromagnetic radiation with energy lower than 100 eV, it is able to extract the valence electrons [26-28]. Due to limitations of the escape depth of electrons in solids, UPS is very surface sensitive, as the information depth is in the range of one mono-layer to 20 nm [29]. The resulting spectrum reflects the electronic structure of the sample, providing information on the density of states, occupation of states, and the work function. However until recently, the family of PES techniques has been limited to uses in ultra-high vacuum (UHV), as the emitted photoelectrons can be easily captured by oxygen molecules in air and only travel a distance less than one centimeter, i.e., the *mean free path of electron in air*.

The UHV constraint that limits the broad use of PES techniques recently has been broken through by the invention of the technique today known as Photoelectron Spectroscopy in Air (PESA) [26-33], which allows direct measuring the work function of a sample exposed to open air, i.e., the service condition of general metallic materials as good conductors. As commonly used metallic materials, both steels and aluminum alloys are metallic materials with overlapped conduction band and valence band [26-28].

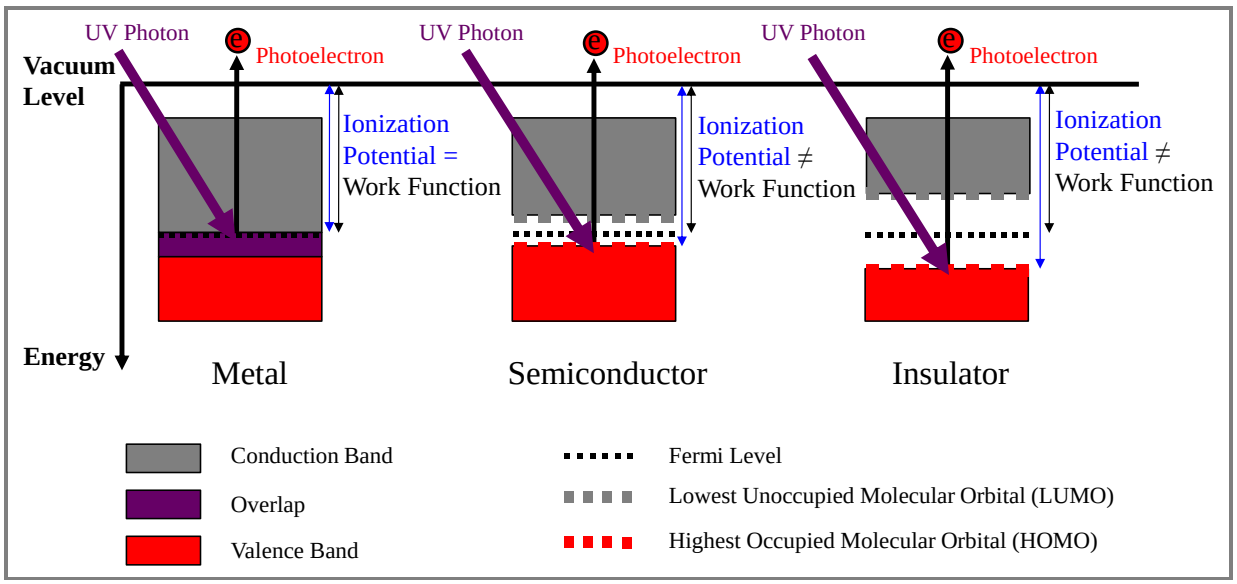

Figure 2. Energy Level Diagrams of Metallic Materials, Semiconductors and Insulators

Figure 2 illustrates the energy level diagrams of different solid-state materials that serve as the theoretical basis of PESA for measuring the work function of solid-state materials [26-33]. Work function is a characteristic property for a solid-state substance with a conduction band whether empty or partly filled. In solid-state physics, the work function is the minimum energy needed to transfer an electron from a solid to a point immediately outside the solid surface, or the energy needed to move an

electron from the Fermi level into vacuum. On the other hand, the ionization potential is an energy difference between a vacuum level and highest occupied molecular orbital (HOMO). According to Figure 2, for a metallic material its Fermi level is inside the conduction band, indicating that the band is partly filled; in insulators however the electrons in the valence band are separated by a large gap from the conduction band. Semiconductors have a small enough gap between the valence and conduction bands that can be bridged up by thermal or other excitations. For semiconductors and insulators, the Fermi level lies within the band gap, indicating an empty conduction band and a work function equal to the sum of half the band gap and the electron affinity.

Incident UV photons can excite an electron in the sample top surface from an occupied state to an energy state higher than the vacuum level, and then the photoelectron can be emitted from the sample surface into the air (see Figure 2). Therefore, the photoemission threshold energy of a solid substance is its ionization potential, according to which the ionization potential of a material can be estimated from the photoemission threshold energy. Metals and alloys are a special type of solid-state material that has the same HOMO and Fermi level; hence the photoemission threshold energy of a metal or alloy is also its work function. This fact is used in PESA to determine the work function of a metallic material, as the photoemission threshold energy of the material can be readily identified by adjusting the energy level of the incident monochromatized UV photons. In PESA, photoelectron spectra by low energy photons are very sensitive to energy change in the HOMO condensed matters; thus compared with other PES techniques such as X-ray Photoelectron Spectroscopy (XPS) and standard UPS, PESA has the advantages of high energy-resolution, in-air measurement, and low photo-excitation energy (therefore non-destructive to sample surface) [26-33].

PESA includes three components: 1) a UV-photon source positioned inside a UV spectrometer, 2) a sample holder, and 3) an open counter. Work function of the tested sample is determined from the photoemission yield, as measured by the open counter, with respect to the incident photon energies generated by the Monochromatized UV photons emitted from the UV-photon source. The open counter is the part that enables the PESA to detect and count photoelectrons in air. The entire UV spectrometer chamber is filled with Nitrogen gas N_2 instead of air to reduce UV-photon absorption. The N_2 gas is introduced into the chamber through the N_2 inlet at a constant flow rate and discharged through the N_2 outlet throughout an experiment. The UV-photons emitted from a deuterium lamp are incident into the chamber through an MgF_2 window and then pass the entrance slit of the spectrometer after being focused by the two concave mirrors. Two concave mirrors and a plane mirror, a diffraction grating are used to further focusing and re-direct the UV-photons before they exit from the slit. The monochromatized UV-photons from the spectrometer were focused by the CaF_2 lens through a CaF_2 window onto the sample surface. The CaF_2 window separates the N_2 filled UV-chamber from the ambient air. The emitted photoelectrons will then be counted by the open counter.

The schematic drawing of the open counter unit of PESA is shown in Figure 3 [26-28]. The open counter consists of an anode wire, a quenching grid built in the inner cylinder, a suppresser grid in the outer cylinder, and a set of electric circuits for controlling the specific potential differences need to accelerating or quenching photoelectrons. The anode is made of gold-plated tungsten wire of 50 μm in diameter. Monochromatized UV photons from the UV-photon source excite photoelectrons from the sample at the earth potential. These electrons are accelerated first by the suppressor grid at + 80 V and

then by the quenching grid at + 100 V. During acceleration, the electrons become attached to O_2 molecules in air and form O_2^- ions, which are then directed into the inner cylinder and further accelerated to the anode by the electric field between the quenching grid at + 100 V and the anode at + 2900 V. When any O_2^- ion arrives near the anode, the electron is detached from the O_2^- ion and then becomes accelerated again towards the anode. Owing to the high potential of the anode wire, the accelerated electron near the anode wire then lead to an electron avalanche that produces many electrons and positive ions around the anode wire, of which only the electrons are collected on the anode. The collected electrons cause an instantaneous voltage reduction in the anode wire that can be detected by the quenching circuit and counted as an electric pulse by one photoelectron entering the counter.

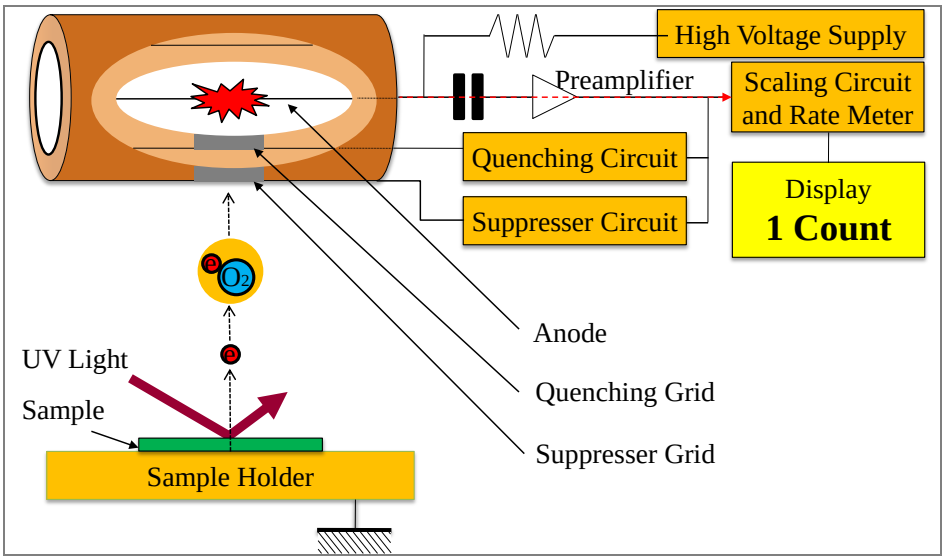

Figure 3. Schematic Illustration of the Open Counter of PESA

$$N_{in} = f \cdot N_{em} = \frac{N_{obs}}{1 - \tau \cdot N_{obs}} \quad (8)$$

As soon as the quenching circuit detects the electric pulse, a + 400 voltage is applied to the quenching grid. Then the electric field around the anode wire is reduced and the gas discharge is quenched. On the other hand, some of positive ions produced around the anode wire could pass through the quenching grid during a quenching. To neutralize these positive ions, a - 30 voltage is applied to the suppressor grid. During the quenching, these positive ions cannot pass through the suppressor grid and the next photoelectron cannot come into the counter. After 3 microseconds, the applied voltages to the quenching grid and suppresser grid are restored to the counter operating condition, i.e., the 100 V and 80 V, respectively. Such a series of voltage-changing procedures prevent successive and continuous gas discharges, and enable photoelectrons in the air to be counted.

The number of counter pulses per second produced at the anode is related to the number of electrons emitted from the sample. A loss of counts, however, may be introduced by presence of the

quenching time of the counter. The number of entered electrons per second into the counter N_{in} can be estimated per Eq. (8) using a phototube placed in the sample position, where N_{em} is the number of emitted electrons per second from the sample, f is the fraction of emitted electrons entering into the counter, τ is the quenching time and N_{obs} is the number of observed electrons per second. The *photoelectric quantum yield* is a calibrated quantity defined by dividing N_{in} by the number of incident photons.

For materials with good conductivity such as general metallic materials, a linear relationship exists between the square root of photoelectric quantum yield and the incident photon energy. By adjusting the energy level of the incident monochromatized UV photons from 0.1 to 7.0 eV, the work function of a metallic material or phase can be determined as the incident photon energy at the inflection point of the square root of photoelectric quantum yield vs. incident photon energy plot, which corresponds to the photoemission threshold energy of the metallic material/phase.

2.3. High-Resolution Measurement of Volta Potential Difference by SKPFM

With the fundamental concepts of work function and absolute electrode potential of metallic materials, the SKPFM was developed based on the techniques of standard SKP and Atomic Force Microscopy (AFM) [34, 35]. The standard SKP consists of a metallic probe (or reference electrode) connected to the sample by a metallic wire; in measurement the probe is positioned near the surface of the sample (see Figure 4-a). The reference electrode and the sample actually form a capacitor in SKPFM; hence, a Volta potential difference per Eq. (9) is established due to the difference of the work functions of sample and reference electrode upon connected by the wire [24, 25].

$$\begin{aligned}\tilde{\mu}_e^{sample} &= \mu_e^{sample} - e\varphi^{sample} = -\Phi^{sample} - e\psi^{sample} \\ &= \tilde{\mu}_e^{Probe} = \mu_e^{Probe} - e\varphi^{Probe} = -\Phi^{Probe} - e\psi^{probe}\end{aligned} \tag{9}$$

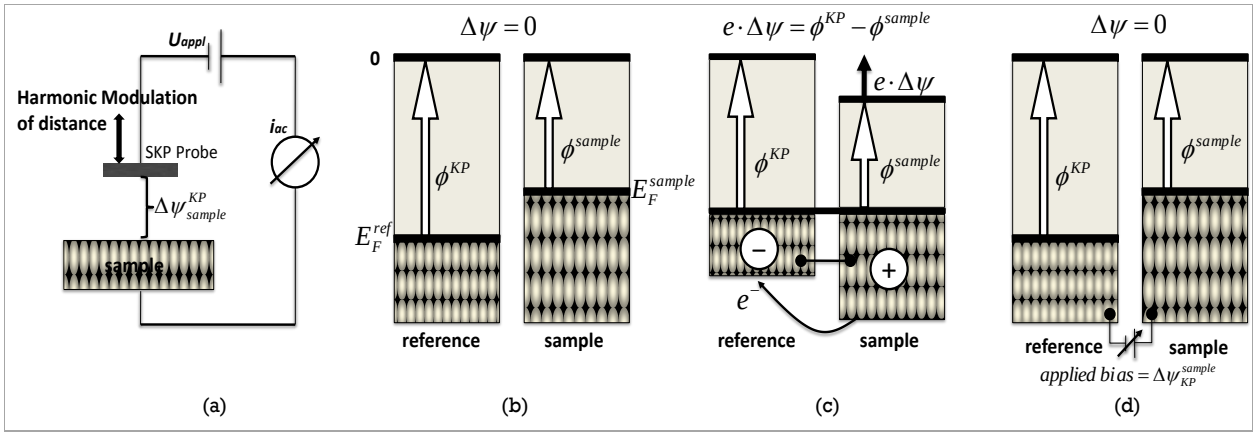

Figure 4. Schematic and Working Principles of Standard Scanning Kelvin Probe

Eq. (9) can be re-organized to be Eq. (10) as follows,

$$e(\psi^{sample} - \psi^{Probe}) = e\Delta\psi_{sample}^{Probe} = \Phi^{Probe} - \Phi^{sample} \quad (10)$$

The difference in work functions between the non-connected reference electrode (i.e., the KP probe that also is a metallic material in Figures 4-b, c and d) and sample is equivalent to the difference in Fermi level positions shown in Figure 4-b. When the reference electrode is connected to the metallic sample, the electrochemical potential $\tilde{u}_e$ of the electrons within the two pieces will be identical and a charging of one piece with respect to the other will occur as shown in Figure 4-c, causing a Volta-potential difference between the reference and sample per Eq. (9), with consideration of $\Phi = -\mu_e + e\chi$. The energetic position of the Fermi level with respect to the absolute vacuum level is given by the electrochemical potential. It is this charging of the capacitor between the reference and sample that is used for measuring the Volta potential difference in SKP (see Figure 4-d) [24, 25, 34, 35].

For a standard SKP probe scanning over the surface of the sample, i.e. the sample-reference distance is periodically modulated at a distance of $d = d_0 + \Delta d \cdot sin(\omega t)$. If the capacitor is expressed in capacitance C as a parallel plate capacitor per Eq. (11), the induced AC current in the external circuit is given in Eq. (12) for $d_0 \gg \Delta d$. The symbol ε is the dielectric constant of the medium, ε_0 is the electric field constant, ω is the frequency of the Kelvin probe vibration, and A is the surface area of the Kelvin probe tip [36-38].

$$C = \varepsilon \cdot \varepsilon_0 \cdot \frac{A}{d_0 + \Delta d\, sin(\omega t)} \quad (11)$$

$$\begin{aligned} i_{ac} &= \Delta\psi_{sample}^{Probe} \cdot \frac{dC}{dt} = \Delta\psi_{sample}^{Probe} \cdot \varepsilon \cdot \varepsilon_0 \cdot \Delta d \cdot \omega \frac{A \cdot cos(\omega t)}{(d_0 + \Delta d\, sin(\omega t))^2} \\ &\approx \Delta\psi_{sample}^{Probe} \cdot \varepsilon \cdot \varepsilon_0 \cdot \Delta d \cdot \omega \frac{A \cdot cos(\omega t)}{(d_0)^2} \end{aligned} \quad (12)$$

If an external voltage U_{appl} is applied between the sample and Kelvin probe (see Figure 4-a), then Eq. (13) is obtained. For the conventional nulling technique in SKP, the voltage U_{appl} is adjusted to get the zero current i_{ac} (see Figure 4-a), and for this condition Volta potential difference $\Delta\psi_{sample}^{Probe} = U_{appl}$ is measured [36-38].

$$i_{ac} = (\Delta\psi_{sample}^{Probe} - U_{appl}) \frac{dC}{dt} \quad (13)$$

Based on the principles of SKP and AFM, the SKPFM technique involves first scanning the sample surface in the AFM tapping mode to determine the topography on a line-by-line basis, and then rescanning across the surface at a fixed height, i.e., in the "lift mode" with the metal-coated or doped silicon cantilever lifted to a fixed distance from the surface, typically 50 to 100 nm, to measure the Volta potential of the sample surface. The tapping piezo is turned off in the rescan, and an AC voltage $V_{ac}sin(\omega t)$ is applied to the tip to stimulate oscillations of the cantilever [34, 35].

The AC voltage $V_{ac}\sin \omega t$ is connected to the Volta potential difference $\Delta\psi$ over the capacitor formed by the SKPFM cantilever/tip and the metallic sample. The magnitude of tip oscillations at the stimulating frequency ω is nulled on a point-by-point basis during the lift mode rescan through adding to the tip a DC voltage V_{dc} that balances the Volta potential difference $\Delta\psi$. Accordingly, unlike the standard SKP that nulls the displacement current, SKPFM nulls the first harmonic of the force exerted by an electric AC field on the charged cantilever/tip. Beyond the nulling mode however, everything concerning the fundamentals of the classical SKP remains valid [34, 35]. The electric energy stored in the capacitor formed by tip/cantilever and sample is given in Eq. (14) in terms of its capacitance C and the potential V of the electrical field in the capacitor per Eq. (15) [34, 35].

$$W_{capacitor} = \frac{1}{2}V^2 C \tag{14}$$

$$V = \Delta\psi - V_{dc} + V_{ac}\, sin(\omega t) \tag{15}$$

The electrical force in the capacitor can be obtained as the gradient of the electric energy $W_{capacitor}$ per Eq. (16).

$$F_e = -\frac{dW_{capacitor}}{dz} = \frac{1}{2}V^2 \frac{dC}{dz} \tag{16}$$

Plugging Eq. (15) in Eq. (16) and considering the trigonometric relation: $\sin^2(\omega t) = \frac{(1-\cos(2\omega t)}{2}$, Eq. (16) eventually turns into Eq. (17) that forms the basis for the nulling mechanism in SKPFM, i.e., by applying a DC voltage V_{dc} between the sample and probe that is equal to the Volta potential difference: $V_{dc} = \Delta\psi_{Sample}^{Probe}$. Therefore, nulling of the force directly yields the measurement of Volta potential difference in SKPFM.

$$F_e = \frac{1}{2}\left(V_{dc} - \Delta\psi_{Sample}^{Probe}\right)^2 \cdot \frac{dC}{dz} + \left(V_{dc} - \Delta\psi_{Sample}^{Probe}\right)\cdot V_{ac}\, sin(\omega t)\cdot \frac{dC}{dz} + \frac{1}{4}\left[V_{ac}^2\, cos(2\omega t) + V_{ac}^2\right]\cdot \frac{dC}{dz} \tag{17}$$

2.4. Coupling PESA and SKPFM Measurements to Obtain E_{abs}

Studying the sub-microscopic mechanisms of corrosion and coating mechanisms entails the coupled use of PESA and SKPFM techniques for measuring the in-situ work potential and the Volta potential difference between the SKPFM probe and metallic surface and the Volta potential difference between SKPFM probe and the surface of liquid covering the metallic material. As most metallic materials used for engineering purposes are composites of multiple metallurgical or compositional phases, the PESA and SKPFM measurements both require special techniques that are described as follows. Notably, this approach involves direct measurements of work function and Volta potential difference that both can be conducted at the sub-microscopic resolution and high accuracy based on the state-of-the-art surface analysis techniques.

Figure 5 illustrates the measurement of work function by PESA on a multi-inclusion metallic surface. For any single solid phase its work function can be determined at the inflection point of its unique linear photoelectron yield vs. incident photon energy relationship. When multiple solid phases are included on a metallic surface, the photoelectron yield vs. incident photon energy relationships, one for each phase, will be overlapped. The individual relationship can be extracted one by one starting from the phase with the lowest work function, by increasing the incident photon energy from 0.1 eV to 7.0 eV. If semi-conductive materials (e.g., iron oxides) or insulators (e.g., aluminum oxides) are involved, their ionization potential can be found in the same way as finding the work function of a conductor [26-33].

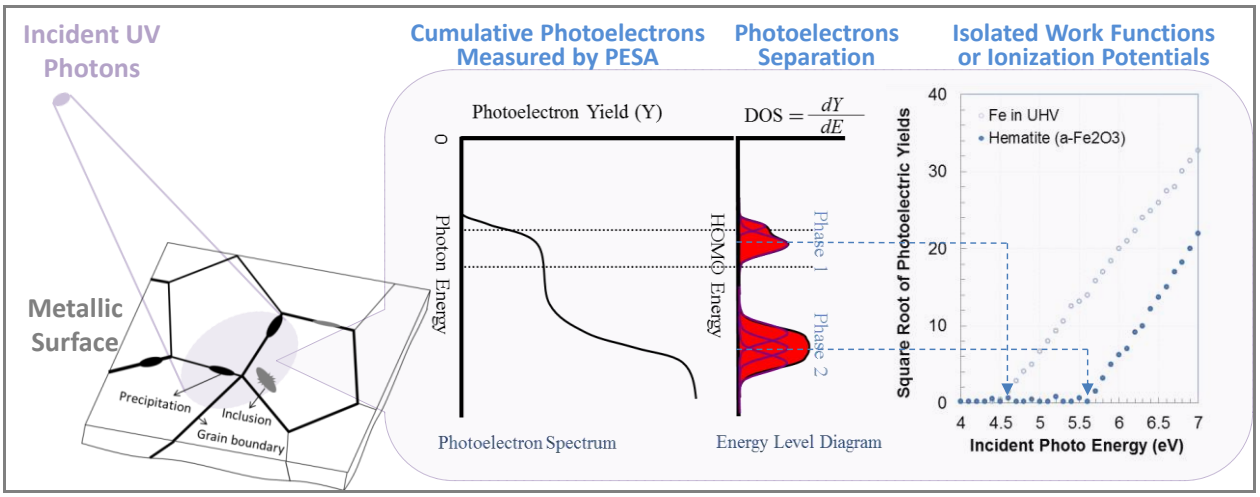

Figure 5. PESA Measurement of Work Function a Multi-inclusion Metallic Surface

An alternate and more efficient way for determining the work functions of a composite surface is by differentiating the cumulative photoelectron yield with respect to the incident photon energy. As illustrated in Figure 5, the two red colored zones represent the HOMO energy levels of two solid phases on one metallic surface. These two phases were first separated by the differentiation technique and then plotted to determine the work functions [26-28]. The determination of work functions or ionization potentials of a multiple-phase surface today can be done automatically by the program that comes with the PESA device. The result of a PESA analysis therefore will be a series of work function or ionization potential values of a metallic surface.

The Volta potential difference terms $(\psi^M - \psi^{Probe})$ and $(\psi^{Probe} - \psi^S)$ need to be measured by SKPFM for determining the absolute electrode potential per Eqs. (7-b) or (7-b-1). The schematic illustration of measuring $(\psi^M - \psi^{Probe})$ and $(\psi^{Probe} - \psi^S)$ by the SKPFM is shown in Figure 6, which entails exposing the metallic surface and liquid surface to the probe tip, respectively.

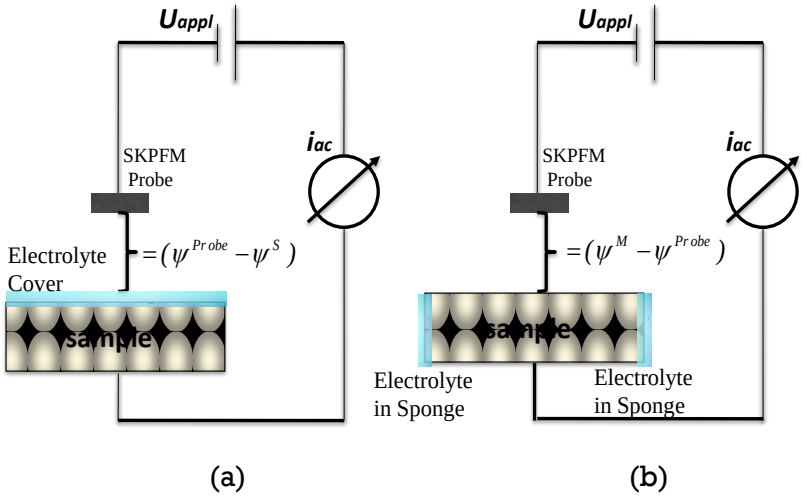

Figure 6. Measurements of Volta Potential Differences $(\psi^{Probe}-\psi^{S})$ and $(\psi^{M}-\psi^{Probe})$ by SKPFM

Figure 7 gives more details regarding the Volta potential difference measurement by SKPFM on a multi-inclusion metallic surface. The scanning movement of the probe tip forms a different capacitor with each different phase of the metallic surface, from which a unique Volta potential difference value is reported. Different from the PESA analysis, the result of SKPFM measurement will be a map showing the Volta potential difference values at the sub-microscopic spatial resolution, like the Volta potential map shown in Figure 7 for a Duplex steel.

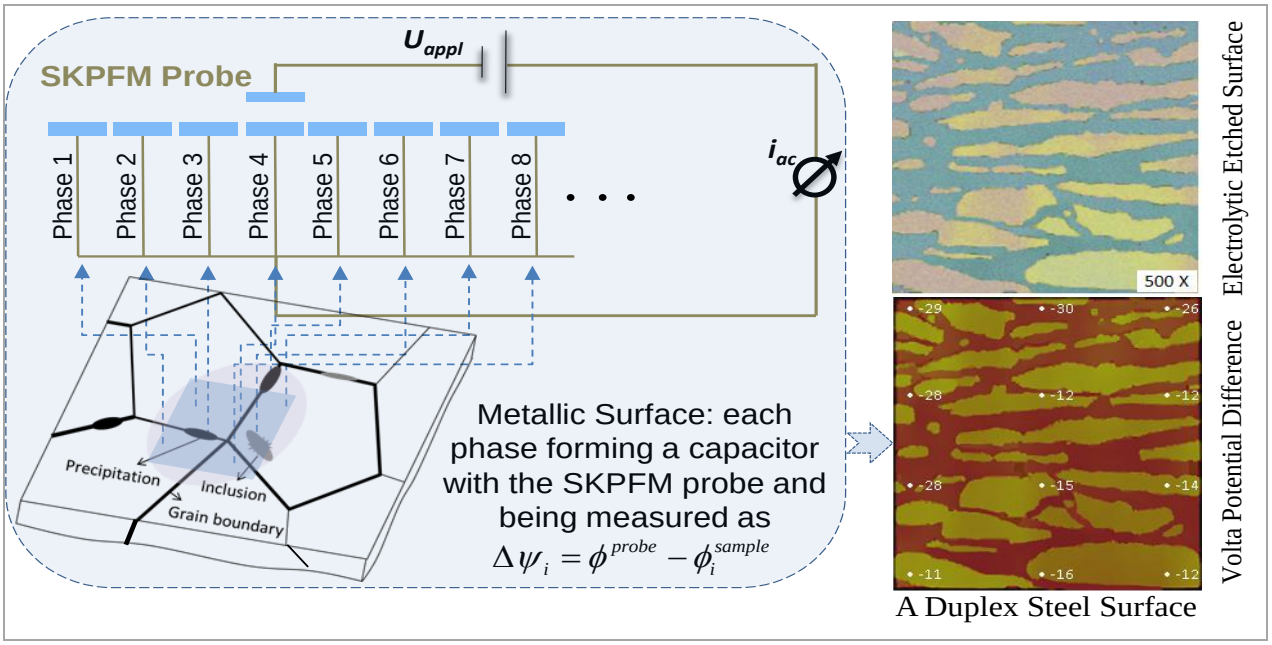

Figure 7. SKPFM-Based Measurement of Volta Potential Difference of a PESA Measured Domain

3. EXAMPLE OF APPLICATION

As an example of implementing the developed approach, the work function of a high-purity iron sample and a high-purity aluminum sample, and the ionized potential of a hematite (□-Fe_2O_3) sample were measured by PESA in both UHV and air at Relative Humidity (RH) of 80% by the PI to examine the electrode potential of the metals at different surface passivation conditions. It is noteworthy that iron oxides are typical semiconductors; while the aluminum oxides, mainly the Al_2O_3, are electrical insulators. Therefore it is the ionization potential instead of the work function that is measured by PESA for these oxides. The PESA data are shown in Figure 8, based on which the work function or ionized potential of the materials are obtained as listed in the second row of Table 1.

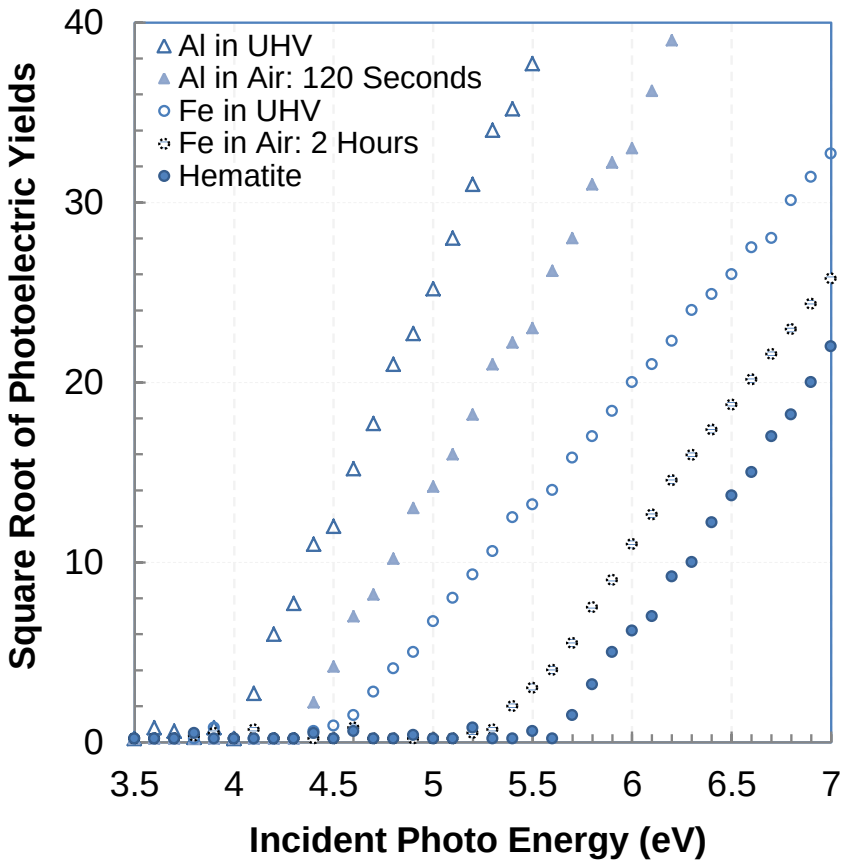

Figure 8. PESA Measured Work Functions of High-Purity Iron and Aluminum and Hematite Samples

From Figure 8, the work functions of aluminum in UHV and in air were determined to be 4.082 eV and 4.331 eV, work functions of iron in UHV and in air were determined to be 4.510 eV and 5.249 eV, and the ionized potentials of hematite (□-Fe_2O_3) in UHV and in air was determined to be 5.632 eV and 5.634 eV. The higher work functions measured in moist air than in UHV for both metals were due to the passivation oxides film formed on the samples' surface and the water molecules and some charged species in air.

Table 1. Work Function/Ionization Potential and Absolute Electrode Potential of Iron, Aluminum and Hematite

Solid–State Material Quantity	Fe in UHV	Fe in Air: 2 hours	Fe_2O_3 in UHV	Fe_2O_3 in Air	Al in UHV	Al in Air: 2 minutes
Work Function or Ionization Potential (eV)	4.510	5.249	5.634	5.632	4.082	4.331
Absolute Electrode Potential by Coupled PESA and SKPFM (V)	4.232	5.123	N/A	N/A	3.872	4.113
Absolute Electrode Potential by SCE Electrode w.r.t. SHE (V)	4.231	5.121	N/A	N/A	3.870	4.111

The Volta potential differences $(\psi^M - \psi^{Probe})$ and $(\psi^{Probe} - \psi^S)$ measured by SKPFM were - 0.049 V and - 0.069 V, and -0.056 V and – 0.070V for the high-purity iron sample in UHV and in air, respectively; and - 0.126 V and - 0.082 V, and -0.135 V and -0.083 V for the high-purity aluminum sample in UHV and in air, respectively. Since the absolute electrode potential is not defined for hematite as a semiconductor, SKPFM was therefore not tried on the hematite sample. The Pt-coated silicon cantilever probe were used as the conductive probe with a force constant of approximately 2–5 N/m and a nominal resonance frequency of 70 kHz. The SKPFM probe tip was positioned 100 nm above the metallic sample for Volta potential measurement. According to Eq. (7-b), the absolute electrode potential E_{abs} of the high-purity iron sample was determined to be 4.232 V (= 4.510 - 0.049 - 0.069) in UHV and 5.123 V (= 5.249 - 0.056 - 0.070) in air, respectively; and of the high-purity aluminum sample to be 3.872 V (= 4.082 - 0.126 - 0.082) in UHV and 4.113 V (= 4.331 – 0.135 – 0.083) in air, respectively, as listed in the fourth row of Table 1.

To validate the innovative approach, the open-circuit potential (OCT) of the high-purity iron and aluminum samples were measured by the standard reference electrode. The standard hydrogen electrode (SHE) has an absolute electrode potential: 4.44 ± 0.02 V at 25º C; practically however it is more convenient to use an alternative electrode whose potentials are precisely known with respect to the SHE. Two of the electrodes most commonly used for this purpose are the saturated calomel electrode (SCE) at + 0.242 V w.r.t. SHE and the Ag/AgCl electrode at + 0.2224 V w.r.t. SHE. The SCE was used in the example, which measured an OCT of – 0.451 V and + 0.439 V for the iron in UHV and in air and – 0.812 V and – 0.571 V for the aluminum in UHV and in Air, respectively. With the absolute electrode potential of SHE, 4.44 V, and the reference electrode potential of SCE w.r.t. SHE, 0.242 V, the absolute electrode potential of the iron sample and were equal to 4.231 V (= 4.44 + 0.242 - 0.451) in UHV and 5.121 V (= 4.44 + 0.242 + 0.439) in air, respectively; and of the aluminum sample to be 3.870 V (= 4.44 + 0.242 - 0.812) in UHV and 4.111 V (= 4.44 + 0.242 – 0.571) in air, respectively as listed in the fourth row of Table 1. These values well match the E_{abs} measurements by the coupled PESA and SKPFM method. It is noteworthy that the conventional reference electrode method is not capable of distinguishing and measuring the electrode potential of the individual phases

(heterogeneities) of a metallic surface. This is why the high-purity iron and aluminum samples were used for the validation purpose in this application example.

4. SUMMARY AND CONCLUSIONS

The current state of knowledge in corrosion management of technically protected metallic materials demands a well-developed capability to precisely track the sub-microscopic corrosion phenomena and enable a quantitative understanding of the mechanisms of corrosion and commonly used protection strategies, which however is beyond the capacities of conventional electrochemical techniques. This study developed an innovative method by directly measuring the absolute electrode potential E_{abs} on a metallic surface that can be accomplished at the atomic-level resolution and accuracy. The absolute electrode potential of a specific solid-state metallic material or phase, which is believed to be practically immeasurable in classical electrochemistry, includes two contributing components, i.e., the work function of the material/phase and the Volta potential difference between the material/phase and the aqueous electrolyte covering its surface. With the state-of-the-art surface analytical techniques, i.e., PESA and SKPFM, the two components can be measured at the atomic-level resolution and accuracy. The coupled PEESA and SKPFM approach allows measuring the absolute electrode potential E_{abs} of a metallic surface covered by oxides, water molecules and/or coating materials and determining the physical changes and integrity of the cover materials (e.g., changes in oxide thickness, coating delamination, etc.), which allows the in-situ studying of sub-microscopic corrosion phenomena under various in-service conditions.

The accurately determined high resolution E_{abs} map of a metallic surface and physical changes in surface oxide film and coatings can be used under all atmospheric, immersed, or alternate immersed conditions to 1) study the mechanisms of a wide spectrum of corrosion phenomena such as pitting and crevice corrosion, 2) monitor the growth and deterioration of passivation oxides or corrosion products (i.e., monitor the corrosion rate), 3) evaluate the stress and strain effects on corrosion, and 4)test the existing and develop new protection strategies. This study will provide insight into the sub-microscopic domain of metallic corrosion and corrosion protection strategies at a level that has not been achieved thus far, and thereby significantly upgrade the knowledge base of corrosion science and generate far-reaching impacts. The newly developed approach was validated and illustrated with an application example by determining the surface absolute electrode potential of iron and aluminum samples under different conditions.

References

1. R.W. Revie and H.H. Uhlig, *Corrosion and Corrosion Control (4th Edi.).* Wiley (2008).
2. R.N. Parkins, *Stress Corrosion Cracking*, in *Uhlig's Corrosion Handbook, (2nd Edi.).* Wiley (2000).
3. P. Leblanc and G.S. Frankel, *J. Electrochem. Soc.* Volume 149, Issues 6, pp. B239-B247 (2002).
4. E. Herzberg, *The Annual Cost of Corrosion for DoD,* 2009 DoD Corrosion Conference (2009).
5. E. Herzberg, *Cost of Corrosion to DoD,* Corrosion Prevention and Control Integrated Product Team, LMI Government Consulting, Maintenance Symposium (Cleared for Public Release) (2010).

6. E. Herzberg et al., *The Annual Cost of Corrosion for Army Ground Vehicles and Navy Ships* (Cleared for Public Release), Report SKT50T1, LMI Government Consulting (2006).
7. United States General Accounting Office, *Defense Management: Opportunities to Reduce Corrosion Costs and Increase Readiness*, GAO Report to Congressional Committees: GAO-03-753 (2003).
8. T. Pan, *Anal. Lett.* (DOI:10.1080/00032719.2012.694944) (2012).
9. P. Schmutz, and G.S. Frankel, *J. Electrochem. Soc.* 145(7) (1998) 2285-2295.
10. C. Senöz, and M. Rohwerder, *Electrochim. Acta.* 56(26) (2011).
11. M. Rohwerder, et al. *Galvatech.* (2001) 585-592.
12. G. Williams, and H.N. McMurray, *J. Electrochem. Soc.* 148(10) (2001).
13. W. Fürbeth, and M. Stratmann, *Corros. Sci.*. 43(2) (2001) 207-227.
14. R.A. Dickie, and F.L. Floyd, (eds.), *Polymeric Materials for Corrosion Control*, ACS, Washington, DC, 1986.
15. S. Trasatti, *Electrochim. Acta.* 36(11-12) (1991) 1659-1667.
16. T. Pan and Y. Lu, *Int. J. Electrochem. Sci.* 6(8) (2011) 4967-4983.
17. T. Pan, *Chem. Phys. Lett.* 511(4-6) (2011) 315-321.
18. T. Pan and A.C.T. van Duin, *Electrocatalysis.* 2(4) (2011) 307-316.
19. T. Pan and Y. Xi, *Acta Metall. Sin*. 24(6) (2011) 415-422.
20. Jr. H. Leidheiser, (ed.), *Corrosion Control by Organic Coatings*, NACE, Houston, USA (1981).
21. F. Martin, et al. *Rev. Sci. Instrum.* 82(12) (2011) 123901.
22. M. Stratmann, R. Feser, and A. Leng, *Elect. Acta.* 39(9) (1994).
23. F. Marcus and F. Mansfeld, (Editor), *Analytical Methods in Corrosion Science and Engineering* (Corrosion Technology), CRC Press (2005).
24. S. Trasatti, International Union of Pure and Applied Chemistry, *Pure and Applied Chemistry*, 58(7) (1986) 955–966.
25. S. Trasatti, *Electrochim. Acta.* 35(1) (1990).
26. H. Kirihata, and M. Uda, *Rev. Sci. Instrum.* 52 (68) (1981).
27. M. Uda, *Japanese Journal of Applied Physics*. 24 (1985) 284.
28. T. Noguch, S. Nagashima, and M. Uda, *Nucl. Instrum. Methods*. Physics A342 (1994) 521.
29. S. Nagashima, T. Tsunekawa, N. Shiroguchi, H. Zenba, and M. Uda, *Nucl. Instrum. Methods*. A373 (1996) 148.
30. A. Koyama, M. Kawai, H. Zenba, Y. Nakajima, A. Yoneda, and M. Uda, *Nucl. Instrum. Methods*. A422 (1999) 309.
31. M. Uda, Y. Nakagawa, T. Yamamoto, M. Kawasaki, A. Nakamura, T. Saito, and K. Hirose, *Journal of Electron Spectroscopy and Related Phenomena*, 88 (1998) 767.
32. Y. Nakajima, M. Hoshino, D. Yamashita, and M. Uda, *Adv. Quantum Chem.* 42 (2003) 399.
33. Y. Nakajima, T. Wakimoto, T. Tuji, T. Watanabe, and M. Uda, *The 10th International Workshop on Inorganic and Organic Electroluminescence*. Hamamatu, Japan. Dec. (2000).
34. M. Nonnenmacher, M.P. O'Boyle, and H.K. Wickramasinghe, *Appl. Phys. Lett.* 58(25) (1991) 2921-2923.
35. M. Nonnenmacher, O. Wolter, J. Greschner, and R. Kassing, *J. Vac. Sci. Technol. B.* 9(2) (1991) 1358-1362.
36. J.H. Parker, and R.W. Warren, *Rev. Sci. Instrum.* 33(9) (1962) 948-950.
37. W. Fürbeth, and M. Stratmann, *Corros. Sci.* 34(2) (2001) 207-227.
38. M. Stratmann, H. Streckel, K.T. Kim, and S. Crockett, *Corros. Sci.* 30(6-7) (1990) 715-734.